Sensor Applications

Deep Learning for Estimating Low-range Concrete Sub-surface Boundary Depths Using Ground Penetrating Radar Signals

Sathira Wickramanayake, Karthick Thiyagarajan* and Sarath Kodagoda*

iPipes Lab, UTS Robotics Institute, Faculty of Engineering and Information Technology, University of Technology Sydney, New South Wales, 2007, Australia.

* *Member, IEEE*

Manuscript received September X, 2021; revised XXX XX, 2021; accepted XXXX, 2022. Date of publication XX xxx, 2021; date of current version XXX XX, 2022.

Abstract—This letter proposes a deep learning approach for non-destructively detecting concrete sub-surface boundaries between corroded and non-corroded layers using ground penetrating radar (GPR). We utilised a finite difference time domain technique to simulate GPR electromagnetic wave propagation on various concrete models mimicking corrosion situations. Following that, a deep learning method based on convolutional neural networks was utilised to estimate the bulk relative permittivity of the compound concrete structure, as well as a multilayer perceptron based method for clutter removal through surface wave prediction. By estimating relative permittivity and removing clutter in GPR signals, the proposed approach can reliably detect the sub-surface boundaries, which was demonstrated by the evaluation results.

Index Terms—Clutter removal, Concrete pipe corrosion, Convolutional neural network, Deep learning, Ground penetrating radar, Infrastructure robotics, Infrastructure sensing, Multilayer perceptron, NDE, Relative permittivity, Smart sensing, Wastewater pipes.

I. INTRODUCTION

Globally, most civil infrastructure in old cities is ageing. Robots are increasingly being used to inspect and renew them. Concrete wastewater pipes are one kind of infrastructure where robots are encouraged since human entry and inspection is too risky. Concrete wastewater pipes age and get corroded [1], causing utilities to spend millions on repairs and replacements [2].

Currently, predictive analytics models are used to indirectly predict corrosion conditions based on multi-sensor monitoring [3]–[6]. This technique, however, requires long-term monitoring of parameters and does not provide a direct assessment of concrete corrosion; furthermore, sensors may fail over time owing to unfavourable environmental conditions [7]. Corrosion can be determined directly by taking core samples [8] or through a drill resistance sensor [9]. But asset inspectors accomplish this manually, and measuring robots have considerable issues related to stability, power requirements, and remote operation. Furthermore, direct measurements cannot be made when the pipe is too small for asset inspectors to enter and inspect. Due to the limits of current technologies, we are working on a non-destructive method for detecting corrosion.

In [10], we showed that Ground Penetrating Radar (GPR) is capable of detecting sub-surface boundaries between corroded and non-corroded concrete layers. When using GPR to estimate the depth or thickness of a material, the relative permittivity, also known as the dielectric constant, is crucial. One method of estimating relative permittivity is hyperbola fitting, which is based on the shape of the hyperbola generated in a GPR B-scan when a surface over a metallic cylinder is scanned. However, this technique necessitates the availability of a circular metallic object under the surface, which must be apparent in the B-scan image, and there must be no air gap between the sensor and the measuring surface. This is not the case in most test situations. Other methods for determining relative permittivity include the reflection coefficient, refraction angles, and the common mid-point theorem. They all need a clear reflection in the B-scan image at a considerable depth below the surface [11].

Another issue with GPR scanning is the clutter in the received signal, which may obscure valuable information. The direct antenna reflection from the transmitter to the receiver (direct-coupling reflection), the reflection of the top surface of the test object, and the ringing effect of the radar signals all contribute to this clutter. Any relevant near-surface reflections will be convoluted by direct coupling and surface wave reflection, making GPR useless for obtaining information about near-surface objects in a compound structure. For any particular antenna, the direct coupling antenna reflection will have a constant waveform, which may be readily eliminated by subtracting a previously collected direct coupling A-scan from the test scan. However, eliminating the surface reflection wave is non-trivial since it changes depending on the surface characteristics. Background subtraction [10] is a popular clutter reduction technique used in GPR testing. This technique eliminates all repeated reflections in a given time frame, and its quality is mostly determined by the sampling window's width. Background subtraction has the drawback of removing all repeated reflections in a scan, which might include reflections from a material layer or a lengthy fracture in a concrete structure at a consistent depth under the surface. In previous studies [12]–[14], deep learning and neural network based methods have been used to estimate GPR traces using numerically modelled GPR antennas, provided that the physical characteristics of the material under observation are known.

This letter proposes a deep learning approach for estimating the bulk relative permittivity of the top layer of a compound material and for filtering out (clutter removal) the direct-coupling (antenna reflections) and the surface reflections from a GPR scan in order to identify the concrete sub-surface boundaries. We have evaluated our proposed method through Finite Difference Time Domain simulations of GPR electromagnetic wave propagation data. The superiority of this technique is that it retains all of the near-surface characteristics of the scan and does not require the use of a surface coupled GPR sensor,

Corresponding author: Karthick Thiyagarajan (e-mail: Karthick.Thiyagarajan@uts.edu.au).
(xxxxxxxxxxxxxxxxxxxxxxxxxxxx).
Associate Editor: XXXXXXXXXX.
Digital Object Identifier: XX

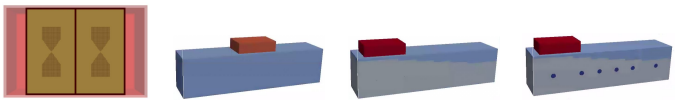

(a) (b) (c) (d)

Fig. 1: Simulation models. (a) The modelled GSSI $1.5GHz$ antenna [15], (b) Model 1, (c) Model 2, (d) Model 3.

which makes it more advantageous for in-pipe robotic inspections.

II. METHODOLOGY

A. Finite Difference Time Domain Simulation of GPR Electromagnetic Wave Propagation

In this work, we use the open-source gprMax software [15] to simulate electromagnetic wave propagation using a pre-built numerical model of the GSSI $1.5GHz$ GPR antenna, which is shown in Fig. 1(a). This realistic Finite-Difference Time-Domain (FDTD) method based 3D antenna model's signals were validated with the commercially available real GPR antenna [12]. The FDTD simulations were done on three different models.

As shown in Fig. 1(b), Model 1 is made of a single piece of concrete material with dimensions of $300mm \times 250mm \times 100mm$, and the GPR antenna is placed in the centre of the top side of the structure. Scans were collected at heights ranging from $0mm$ to $50mm$ above the top surface. A series of A-scans were acquired for each model at intervals of $10mm$ as the antenna was moved horizontally over the concrete surface. The target application for this work is corrosion monitoring of sewer walls. In most situations, the corrosion layer is soft, uneven, and mushy, presenting problems in robotic sensing applications when the GPR antenna is in direct contact with the surface; therefore, our approach is to maintain the GPR antenna at a certain distance from the measuring surface during the inspection procedure. As the GPR will be integrated with a floating robot platform that moves erratically in response to wastewater flow disturbances, it is non-trivial to maintain a stable distance between the GPR antenna and the concrete surface. Therefore, we obtained data at various heights in order to account for any possible change in distances. This was done for relative permittivity (ϵ_r) values of the material ranging from 4 to 12 with 1-point intervals. Model 2 as shown in Fig. 1(c) is made up of two layers, each with a different ϵ_r value and depth of the first layer increasing from $5mm$ to $40mm$ with $5mm$ steps. The A-scans were obtained at varying heights identical to Model 1 and the top layer's ϵ_r value ranging from 4 to 12 between each scan. The A-scans in model 2 contains the reflections from the interface between two layers. Model 3 was developed similar to Model 2, but it has embedded reinforcing bars ($20mm$ diameter) within the bottom layer, which is similar to a real concrete wastewater pipe. The overall dimensions of Model 2 and Model 3 are similar to Model 1. The ϵ_r values were chosen to reflect concrete ϵ_r ranges from 4 (dry concrete) to 12 (fully saturated concrete) [16]. As training labels, Model 1 collected surface reflection waveforms for various ϵ_r values and heights, whereas Models 2 and 3 collected input features for deep learning models.

For all the models, the environment was spatially discretized into $2mm$ cells in the x, y and z directions with a domain size of $640mm \times 148mm \times 334mm$ surrounded by a Perfectly Matched Layer (PML) boundary region. The ϵ_r value of air and rebars in the simulation model was fixed at 1. The conductivity of concrete, air and rebars was set to $0.042S/m$, $0S/m$ and $1 \times 10^7 S/m$ respectively and the permeability of concrete, air and rebars was set to 1, 1 and 100 respectively. The 3D simulations with the simulated antenna and concrete samples were performed to mimic real-world wastewater concrete pipes. During early testing, we performed all of the simulations with a $1mm$ resolution, after which we repeated all of the simulations with a $2mm$ resolution. Both cases produced approximately similar results; hence, we chose to continue with a $2mm$ resolution to keep computational time minimum.

(a) (b)

Fig. 2: Pre-processed GPR data. (a) The scaled binary image of an A-scan, (b) The spectrogram image of an A-scan.

B. Pre-possessing of GPR Signals

Direct coupling and surface reflection waves are always present in the initial part of an A-scan, which is followed by any sub-surface reflections. Before performing any further pre-processing, the direct coupling reflection was eliminated by removing a previously acquired direct coupling antenna signal from all of the A-scans in the data set. The simulation's output A-scans contained 1558 data points with a total time interval of $6ns$. The first set of images were binary images of each A-scan, which were created by plotting the signal and then converting it to black and white images as shown in Fig. 2(a). The spectrograms of each A-scan (Fig. 2(b)), which depict the spectrum of the signal's frequencies as they change over time, were the second set of images. To decrease the computational burden during model training and prediction, all of the images were resized to a 64×64 size. The output signal from the surface reflection prediction model should closely correlate with the input A-scan, therefore, the input A-scans were fed as a numerical array instead of images for surface wave prediction. Before being fed into the model, the input A-scans were down-sampled to 300 samples using decimation with an integer factor.

C. Deep Learning Approach

In this study, we used two different deep learning techniques. The first model uses a neural network architecture that is made up of two convolutional neural network (ConvNet) branches, for estimating the top layer's ϵ_r. One ConvNet branch takes the A-scan binary image as the input and the other takes the spectrogram image as the input. The two branches are then concatenated producing fully connected layers with Rectified Linear Unit (Relu) activation to form a multi-input model. After feature extraction, the number of neurons in each layer was determined heuristically. The output layer contains linear activation estimates ϵ_r value. The deep learning model for estimating ϵ_r is illustrated in Fig. 3.

The second model is for predicting the surface reflection waveform. The predicted surface wave can be used to remove the surface

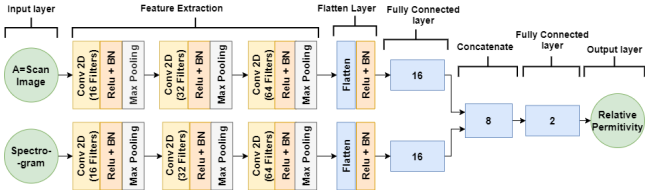

Fig. 3: Relative permittivity estimation model. The numbers in the blocks represent the number of neurons

reflections from a GPR scan without losing any useful near-surface reflections of a scan. The surface reflection waveform prediction model consists of two multilayer perceptron (MLP) branches. One of which accepts the ϵ_r values as the input followed by two Relu activation layers with 40 and 20 neurons respectively, while the other takes the array of the pre-processed A-scan. The MLP branch accepting the pre-processed A-scan signal begins with a Relu activation layer with 600 neurons (twice the size of the input signal) followed by a second Relu activation layer with 400 neurons. The two branches are concatenated, forming 420 neurons, followed by a fully connected layer with 400 neurons and linear activation at the output. The output from this model is the predicted A-scan signal of the surface reflection related to the input signal. The MLP branches consist of fully connected input layers followed by hidden dense layers. The ConvNet branches for image handling consist of convolution, relu activation, batch normalisation, and max pooling layers. The deep learning model for surface wave prediction is illustrated in Fig. 4.

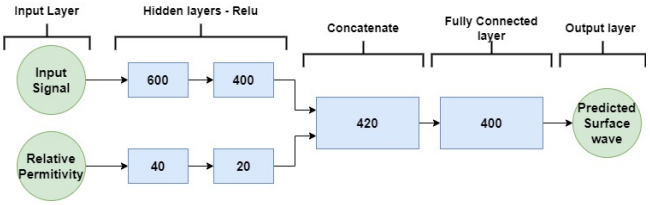

Fig. 4: Surface wave prediction model. The numbers in the blocks represent the number of neurons.

III. RESULTS

A. Relative Permittivity Estimation

Using data collected from the FDTD simulations, the ϵ_r estimation deep learning model was assessed. Out of the 90,558 A-scans collected, 80% of the data was used for training and 20% of the data was used for testing. The test A-scan signals were first pre-processed before being fed into the model. The model was evaluated using 18,110 randomly selected test data samples that were not involved during the training process. The Adam optimizer with a learning rate of 0.0001 was used to train this model with Mean Absolute Error (MAE) as the loss function and a batch size of 32. The training was done until the loss curve stopped improving. The estimated results were plotted against the true ϵ_r values, which is illustrated in Fig. 5(a) that shows the effectiveness of the estimation. Fig. 5b shows the frequency of occurrence of ϵ_r with respect to the absolute error of prediction. Over 70% of the estimated results have an absolute error of less than 0.25, and 99% of the predictions have an absolute error of less than 1. The validation MAE was 0.19, which shows that the accuracy of ϵ_r estimation is high for the proposed technique.

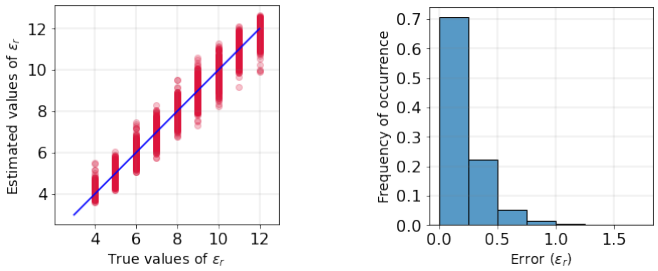

(a) (b)

Fig. 5: Relative permittivity estimation. (a) Estimated ϵ_r versus true ϵ_r values and (b) Error frequency of occurrence.

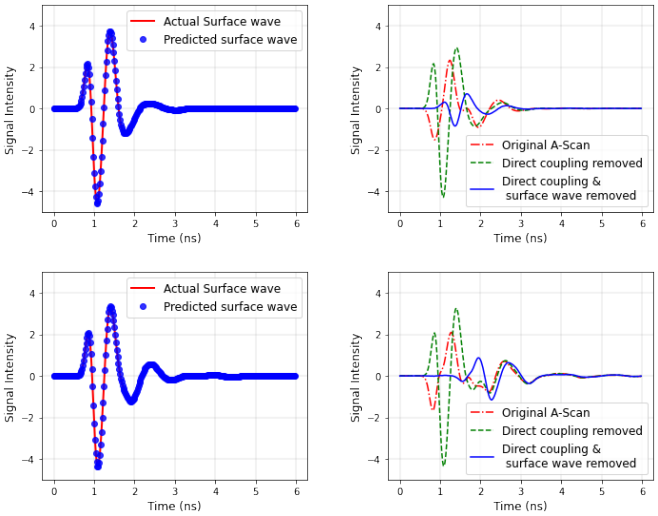

Fig. 6: Comparison of the predicted surface wave with the test data.

B. Surface Wave Prediction

After estimating the ϵ_r of the test object's top layer, we input this estimated value, together with the original A-scan, into the surface wave prediction model to obtain the A-scan of the surface reflection. The model was trained using 72,448 data samples and evaluated using 18,110 test data samples. The Adam optimizer with a learning rate of 0.0001 was used to train this model with Mean Squared Error (MSE) as the loss function and a batch size of 32. The training was done until the loss curve stopped improving. The validation MSE was 0.0013, which is quite low, indicating the accuracy of the proposed model. Fig. 6 shows the comparison of the predicted surface wave with the true surface wave for a few randomly selected test data. Filtering out the direct coupling and the surface wave from the original A-Scan of the test data results in an A-Scan signal with clear reflections from only the sub-surface features and boundaries in the test object.

C. Sub-surface Boundary Detection & Depth Estimation

The velocity (v) of GPR signals in the material can be determined by $v = \frac{c}{\epsilon_r}$ using the estimated value of relative permittivity (ϵ_r) and the speed of light in a vacuum (c). The computed v can then be used to calculate the depth (d) of a sub-surface boundary through the equation $d = \frac{v \times T}{2}$, where T is the two way travel time of the boundary reflection, obtained using the filtered B-scan. A simulation

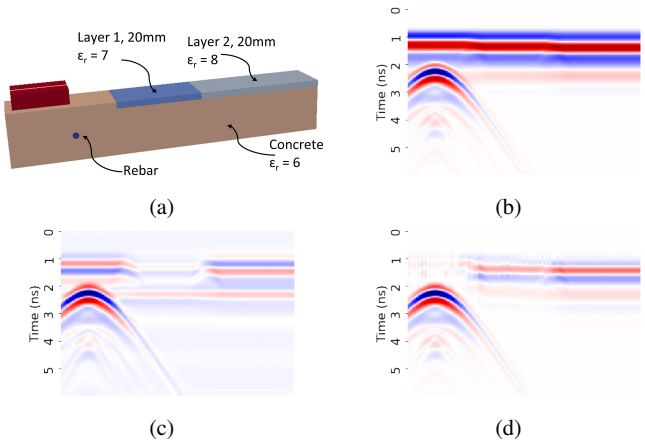

Fig. 7: Evaluation of the concrete with sub-surface layers and a rebar. (a) Simulator model to evaluate boundary and depth determination, (b) Original B-Scan, (c) B-Scan filtered using conventional background subtraction, and (d) B-Scan filtered using the proposed method.

was performed on a model resembling a concrete slab with one reinforcing bar (rebar) and concrete corrosion on top represented by two layers of different materials on the surface at a thickness of $20mm$, as illustrated in Fig. 7(a). A B-scan of the sample was generated by collecting a series of A-scans at $2mm$ intervals with a fixed height of $5mm$ along the surface. The individual A-scans from the evaluation model were fed into the two deep learning models to get the ϵ_r of the top layer and the surface wave at every location of the scan. The predicted surface reflection waveforms were subtracted from each direct coupling removed A-scan of the scan data. The resulting B-scan shown in Fig. 7(d), filtered using the proposed method, shows reflections at the layer boundaries and shows no reflections in the area above the rebar where no different material layers were present. In contrast, the B-scan shown in Fig. 7(c), filtered using conventional background subtraction, still shows the surface reflections in the area above the rebar and the layer boundary reflections are partially convoluted with the surface reflection.

IV. DISCUSSION

We are currently developing a robot for assessing corrosion in wastewater pipelines using GPR scans. We intend to combine simulated and real data from the pipes in the future to improve the proposed deep learning framework for determining the corroded concrete sub-surface boundary depths. The adoption of minimum signal processing-based approaches such as in [17] was not an option for measuring the concrete corrosion depths since the features in a GPR signal depend not only on factors that correlate to the thickness of corrosion but also on other factors, including surface conditions and material composition of concrete, making it difficult to identify a significant feature in a GPR signal to estimate the corrosion levels using minimal signal processing techniques.

V. CONCLUSION AND FUTURE WORK

In this letter, we have presented a novel deep learning approach to detect the concrete sub-surface boundaries by taking GPR non-destructive measurements. This is achieved by utilising ConvNet and MLP based deep learning techniques to estimate the bulk relative permittivity of the top layer and the surface reflection of a concrete structure. The proposed method allows GPR B-scan images to be filtered to enhance the reflections from the low-range boundaries present in the concrete that are usually convoluted by direct coupling and surface reflection. We have evaluated the proposed deep learning approach efficacy with the FDTD simulated GPR data, and the results demonstrate the high accuracy of the proposed method. This work will be extended by utilising a physical GPR antenna to gather real-world A-scan signals, and the proposed method will be applied to the obtained data to determine the depth of the corroded layer.

REFERENCES

[1] A. Gunatilake, L. Piyathilaka, A. Tran, V. K. Vishwanathan, K. Thiyagarajan, and S. Kodagoda, "Stereo vision combined with laser profiling for mapping of pipeline internal defects," vol. 21, no. 10, pp. 11 926–11 934, May 2021.

[2] B. Rente, M. Fabian, Y. Chen, L. Vorreiter, H. Bustamante, T. Sun, and K. T. V. Grattan, "In-sewer field-evaluation of an optical fibre-based condition monitoring system," *IEEE Sensors Journal*, vol. 20, no. 6, pp. 2976–2981, Mar. 2020.

[3] M. M. Montazeri, N. D. Vries, A. D. Afantchao, A. O'Brien, P. Kadota, and M. Hoorfar, "Development of a sensing platform for nuisance sewer gas monitoring: Hydrogen sulfide detection in aqueous versus gaseous samples," *IEEE Sensors Journal*, vol. 18, no. 19, pp. 7772–7778, Oct. 2018.

[4] K. Thiyagarajan, S. Kodagoda, R. Ranasinghe, D. Vitanage, and G. Iori, "Robust sensing suite for measuring temporal dynamics of surface temperature in sewers," *Scientific Reports*, vol. 8, no. 1, Oct. 2018.

[5] B. Rente, M. Fabian, M. Vidakovic, L. Vorreiter, H. Bustamante, T. Sun, and K. T. V. Grattan, "Extended study of fiber optic-based humidity sensing system performance for sewer network condition monitoring," *IEEE Sensors Journal*, vol. 21, no. 6, pp. 7665–7671, Mar. 2021.

[6] K. Thiyagarajan, S. Kodagoda, R. Ranasinghe, D. Vitanage, and G. Iori, "Robust sensor suite combined with predictive analytics enabled anomaly detection model for smart monitoring of concrete sewer pipe surface moisture conditions," *IEEE Sensors Journal*, vol. 20, no. 15, pp. 8232–8243, Aug. 2020.

[7] K. Thiyagarajan, S. Kodagoda, L. V. Nguyen, and R. Ranasinghe, "Sensor failure detection and faulty data accommodation approach for instrumented wastewater infrastructures," *IEEE Access*, vol. 6, pp. 56 562–56 574, 2018.

[8] S. Taheri, M. Ams, H. Bustamante, L. Vorreiter, M. Withford, and S. M. Clark, "A practical methodology to assess corrosion in concrete sewer pipes," *MATEC Web of Conferences*, vol. 199, no. 06010, p. 4, 2018.

[9] N. Giovanangeli, L. Piyathilaka, S. Kodagoda, K. Thiyagarajan, S. Barclay, and D. Vitanage, "Design and development of drill-resistance sensor technology for accurately measuring microbiologically corroded concrete depths," in *2019 Proceedings of the 36th ISARC*. IAARC, May 2019, pp. 735–742.

[10] N. Ulapane, L. Piyathilaka, and S. Kodagoda, "Some convolution and scale transformation techniques to enhance GPR images," in *2019 14th IEEE Conference on Industrial Electronics and Applications*. IEEE, Jun. 2019, pp. 1453–1458.

[11] S. Serkan and V. Borecky, "Estimation methods for obtaining GPR signal velocity," *International Journal of Civil Structural Engineering*, vol. 3, no. 1, pp. 59 – 63, Oct. 2016.

[12] C. Warren and A. Giannopoulos, "Simulating commercial gpr antennas: How close can we get?" 06 2012.

[13] J. K. Alvarez, S. Sutjipto, and S. Kodagoda, "Validated ground penetrating radar simulation model for estimating rebar location in infrastructure monitoring," in *2017 12th IEEE Conference on Industrial Electronics and Applications*. IEEE, Jun. 2017, pp. 1460–1465.

[14] I. Giannakis, A. Giannopoulos, and C. Warren, "A machine learning approach for simulating ground penetrating radar," in *2018 17th International Conference on Ground Penetrating Radar (GPR)*. IEEE, Jun. 2018, pp. 1–4.

[15] C. Warren, A. Giannopoulos, and I. Giannakis, "gprMax: Open source software to simulate electromagnetic wave propagation for ground penetrating radar," *Computer Physics Communications*, vol. 209, pp. 163–170, Dec. 2016.

[16] A. Ogunsola, U. Reggiani, and L. Sandrolini, "Shielding effectiveness of concrete buildings," in *IEEE 6th International Symposium on Electromagnetic Compatibility and Electromagnetic Ecology, 2005.*, 2005, pp. 65–68.

[17] D. Tamhane, J. Patil, S. Banerjee, and S. Tallur, "Feature engineering of time-domain signals based on principal component analysis for rebar corrosion assessment using pulse eddy current," *IEEE Sensors Journal*, vol. 21, no. 19, pp. 22 086–22 093, 2021.